AEROSPACE NUCLEAR SAFETY

RESEARCH REPORT

DRAG COEFFICIENTS AND HEATING RATIOS FOR RIGHT CIRCULAR CYLINDERS IN FREE-MOLECULAR AND CONTINUUM FLOW FROM MACH 10 TO 30

R. D. Klett, 9312

SC-RR-64-2141

SANDIA CORPORATION

PRIME CONTRACTOR TO THE UNITED STATES ATOMIC ENERGY COMMISSION

ALBUQUERQUE, NEW MEXICO

LIVERMORE, CALIFORNIA

DISCLAIMER

SC-RR-64-2141

DRAG COEFFICIENTS AND HEATING RATIOS FOR RIGHT CIRCULAR CYLINDERS IN FREE-MOLECULAR AND CONTINUUM FLOW FROM MACH 10 TO 30

Robert D. Klett, 9312
Sandia Laboratory, Albuquerque

ABSTRACT

Methods are presented for calculating drag coefficients and average heating ratios for L/D ratios up to 20 and Mach numbers from 10 to 30. The cases of end-on, side-on, end-over-end tumbling, and random tumbling are covered for free-molecular and laminar continuum flow.

December 1964

Issued by Sandia Corporation,
a prime contractor to the
United States Atomic Energy Commission

TABLE OF CONTENTS

LIST OF TABLES

LIST OF ILLUSTRATIONS

LIST OF ILLUSTRATIONS
(Cont)

DRAG COEFFICIENTS AND HEATING RATIOS FOR RIGHT CIRCULAR CYLINDERS IN FREE-MOLECULAR AND CONTINUUM FLOW FROM MACH 10 TO 30

Introduction

Recently it has become necessary to study the effects of re-entry heating on aerospace nuclear power supplies. Basically these power supplies are irregular in shape and do not lend themselves to purely analytical analysis, but several parts of the generators, such as fuel rods and core vessels, are cylindrical in shape. The cylindrical parts can be handled analytically when detached from the generators or when they are in areas where flow is independent of the rest of the generator. Much of the theory as applied to cylinders has been verified by experiment. However, there is some dispersion in the experimental data. Because of this scatter, the methods presented here should be considered only as approximations. When more accuracy is required, experimental studies duplicating flight conditions, L/D ratios, and angles of attack may be necessary.

The model shown in Figure 1 will be used throughout this report.

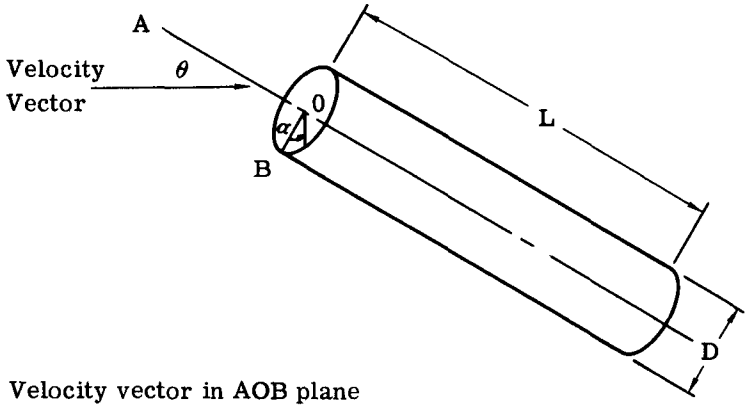

Velocity vector in AOB plane

α measures radial angle with respect to the velocity vector (not applicable when $\theta = 0$ or 180°)

θ measures the angle between the center line of the cylinder and the velocity vector

Figure 1. Cylinder showing angle of attack (θ) and radial angle (α) with respect to the free-stream velocity vector

Drag Coefficients

The projected area of a cylinder in cross flow (LD) will be used as the reference area for all the cases presented. A standard reference area is more convenient for comparison and is necessary for calculating drag coefficients of tumbling bodies.

Free-Molecular Flow

Henry[1] estimates the average velocity of air molecules at high altitudes to be 4900 ft/sec. This is less than one-fifth the velocity of a satellite entering from a circular orbit. Assuming the air molecules striking the vehicle lose all of their kinetic energy to the vehicle and are reflected at roughly the same temperature as the vehicle, the reflected particles should have velocities in the neighborhood of 3000 to 4000 ft/sec. Since the speed of the air molecules before and after their collision with the vehicle is much less than that of the vehicle, it can be concluded that the molecules' incident relative velocity is approximately equal to the vehicle's velocity, and they rebound with a zero relative velocity. The change in momentum of all the air molecules striking the vehicle per unit time is $\rho A V_\infty^2$, (see p. 35 for a listing of the symbols used in this report), which is the drag on the vehicle. Since C_D is defined as (drag)/(dynamic pressure x area), C_D for free-molecular flow is 2, based on the projected frontal area of the vehicle. This figure was derived assuming diffuse reflection and an accommodation coefficient of one. Since diffuse reflection is more probable than spectral reflection, and accommodation coefficients for most materials vary from 0.87 to 0.98, these assumptions do not introduce significant error.

Side-On -- When a cylinder enters stably at $\theta = 90°$, C_D is equal to 2, since the reference area chosen (LD) equals the projected area of the cylinder. This case also represents a cylinder tumbling in a plane perpendicular to the trajectory path.

End-On -- C_DA for a stable cylinder with $\theta = 0°$ is equal to $2\pi R^2$. Converting the drag coefficient to a reference area of LD,

$$C_D = 2\frac{\pi D^2}{4LD} ; \tag{1}$$

hence,

$$C_D = 1.57 \frac{D}{L} . \tag{2}$$

End-Over-End Tumbling -- The average drag coefficient $\overline{C}_D$ will be developed assuming the cylinder is tumbling at a constant angular velocity which is negligible compared to re-entry velocity but sufficient to permit using an average drag coefficient in trajectory calculations.

A_1 = the area of an end (πR^2) and A_2 = the projected side area (LD). Referring to Figure 2, the projected area as a function of θ is

$$A_\theta = A_1 \cos\theta + A_2 \sin\theta \tag{3}$$

and the average C_DA product would be

$$\overline{C}_DA = \frac{\int_o^{\frac{\pi}{2}} C_DA_\theta \, d\theta}{\int_o^{\frac{\pi}{2}} d\theta} . \tag{4}$$

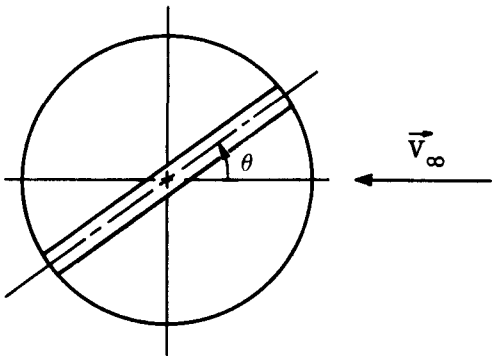

Figure 2. End-over-end tumbling

Substituting Equation 3 into Equation 4 and integrating,

$$\overline{C}_D A = \frac{1}{\pi}(4LD + \pi D^2) \quad . \tag{5}$$

Then for $A_R = LD$,

$$\overline{C}_D = 1.273 + \frac{D}{L} \quad . \tag{6}$$

Random Tumbling -- For this case, it is assumed the cylinder has an equal probability of being aligned in any direction relative to the flight path and changing direction rapidly enough so that an average value of C_D can be used. Using the same nomenclature as for the end-over-end tumbling case, the projected area is again

$$A_\theta = A_1 \cos\theta + A_2 \sin\theta \quad . \tag{7}$$

Referring to Figure 3, the $\overline{C}_D A$ product can be seen to be

$$\overline{C}_D A = \frac{\int_0^{\frac{\pi}{2}} (C_D A_\theta) 2\pi \sin\theta \, d\theta}{\int_0^{\frac{\pi}{2}} 2\pi \sin\theta \, d\theta} \quad . \tag{8}$$

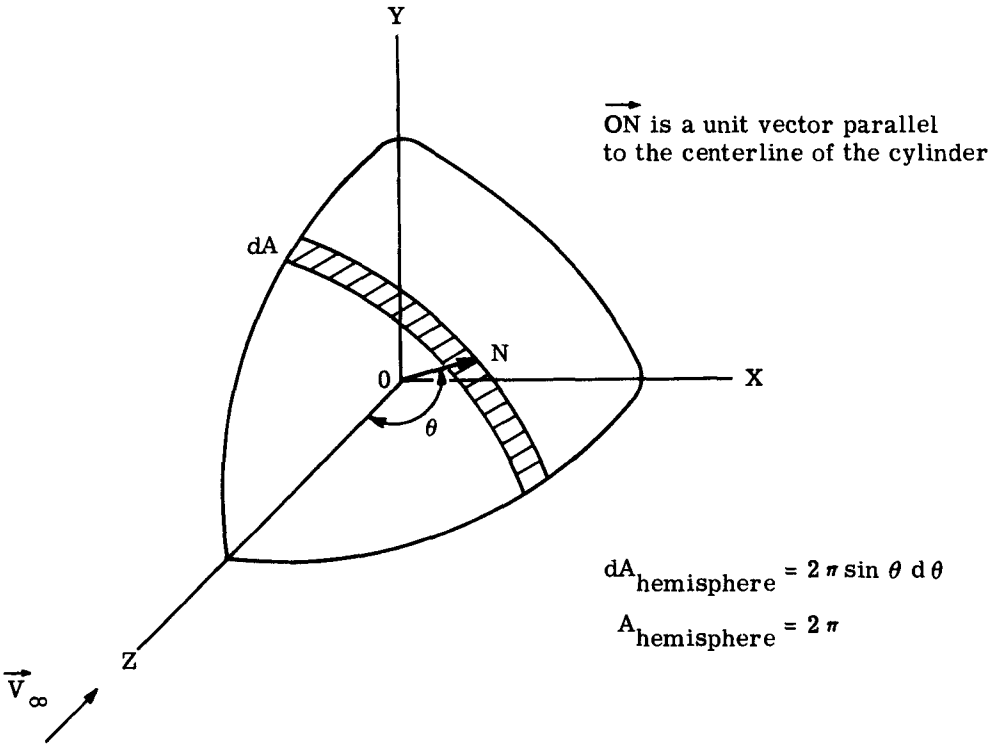

Figure 3. Random tumbling

Substituting Equation 7 into Equation 8 and simplifying,

$$\bar{C}_D A = 2\int_o^{\frac{\pi}{2}} (A_2 \sin^2\theta + A_1 \sin\theta \cos\theta)d\theta \, . \tag{9}$$

Carrying out the integration,

$$\bar{C}_D A = 2\left[A_2(\tfrac{1}{2}\theta - \tfrac{1}{4}\sin 2\theta) + A_1(\tfrac{1}{2}\sin^2\theta)\right]_o^{\frac{\pi}{2}} \tag{10}$$

$$\bar{C}_D A = \frac{\pi LD}{2} + \frac{\pi D^2}{4} \, . \tag{11}$$

Then for $A_R = LD$,

$$\bar{C}_D = 1.57 + 0.785\,\frac{D}{L} \, . \tag{12}$$

Continuum Flow

In Reference 2, Randall developed a method for predicting the drag coefficients of end-on, side-on, and end-over-end tumbling cylinders. A summary of his work will be presented here, along with a procedure for predicting $\bar{C}_D$ for a randomly tumbling cylinder.

For the purpose of this study, it is assumed that there is a modified Newtonian pressure distribution such that the local pressure is given by

$$P = P_\infty + (P_{O_2} - P_\infty) \cos^2 \phi \ . \tag{13}$$

The continuity and momentum equations across a normal shock are

$$\rho_\infty V_\infty = \rho_2 V_2 \tag{14}$$

$$P_\infty + \rho_\infty V_\infty^2 = P_2 + \rho_2 V_2^2 \ . \tag{15}$$

Since incompressible flow relations closely approximate actual conditions in the stagnation region behind the shock wave, Bernoulli's equation may be used. Hence,

$$P_{O_2} = P_2 + \tfrac{1}{2}\rho_2 V_2^2 \ . \tag{16}$$

Combining equations 13, 14, 15, and 16,

$$P = P_\infty + q_\infty \left(2 - \frac{\rho_\infty}{\rho_2}\right) \cos^2 \phi \ . \tag{17}$$

For Newtonian flow, the drag coefficient is given by

$$C_D = \frac{\int P \cos \phi \, dA}{q_\infty A_R} \ , \tag{18}$$

which is integrated over the surface of the body exposed to the free stream. Combining Equations 17 and 18 and making the substitution $K = (\rho_\infty)/(\rho_2)$,

$$C_D = \frac{P_\infty}{q_\infty A_R} \int \cos \phi \, dA + \frac{2 - K}{A_R} \int \cos^3 \theta \, dA \ , \tag{19}$$

which is the general form of the drag coefficient equation in Newtonian flow.

Side-On -- For this case, $dA = L\,(D/2)\,d\phi$ and $A_R = LD$. Substituting into Equation 19 and integrating,

$$C_D = \frac{P_\infty}{q_\infty} + \frac{2}{3}(2 - K) \ . \tag{20}$$

For Mach numbers greater than 10 and altitudes from 70,000 feet to 250,000 feet, $(P_\infty)/(q_\infty)$ is less than 0.012 times the $(2/3)(2 - K)$ term. Therefore the $(P_\infty)/(q_\infty)$ term can be neglected, simplifying Equation 20 to

$$C_D = \frac{2}{3}(2 - K) \ . \tag{21}$$

End-On -- According to Newtonian theory, there would be a uniform pressure P_{o_2} over the face of the cylinder. However, Stoney and Swanson[3] found that the average pressure on the face of a cylinder is 0.909 times stagnation pressure. Using this value in Equation 18 and integrating,

$$C_D = 0.909\left[\frac{P_\infty}{q_\infty} + (2 - K)\right] \ , \tag{22}$$

where the reference area is πR^2. Converting to the standard reference area of LD and neglecting the $(P_\infty)/(q_\infty)$ term,

$$C_D = 0.909(2 - K)\frac{\pi}{4}\frac{D}{L} = 0.714\frac{D}{L}(2 - K) \ . \tag{23}$$

End-Over-End Tumbling -- The same assumptions and nomenclature will be used here as for free-molecular, end-over-end tumbling. In addition, it is assumed that when the cylinder is at an angle of attack, the total drag force is the vector sum of the axial and transverse components. Referring to Figures 2 and 4,

$$\text{Drag} = D_T \sin\theta + D_A \cos\theta \ , \tag{24}$$

or

$$C_{D\theta} q_\infty A_R = C_{DT} q_T A_R \sin\theta + C_{DA} q_A A_R \cos\theta \ . \tag{25}$$

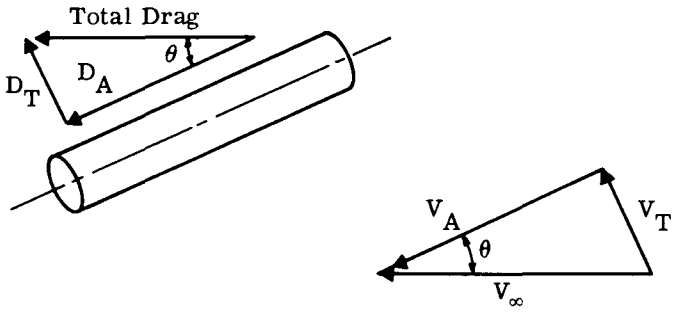

Figure 4. Velocity and drag components

But

$$q_T = \frac{1}{2}\rho_\infty V_T^2 = q_\infty \sin^2\theta \tag{26}$$

and

$$q_A = \tfrac{1}{2}\rho_\infty V_A^2 = q_\infty \cos^2 \theta \ . \tag{27}$$

Substituting Equations 26 and 27 into 25,

$$C_{D\theta} = C_{DT} \sin^3 \theta + C_{DA} \cos^3 \theta \ . \tag{28}$$

Taking C_{DT} and C_{DA} from Equations 21 and 23 respectively,

$$C_{D\theta} = \left[\tfrac{2}{3}(2 - K)\right] \sin^3 \theta + \left[0.714\tfrac{D}{L}(2 - K)\right] \cos^3 \theta \ . \tag{29}$$

The average drag coefficient for end-over-end tumbling can then be found by

$$\overline{C}_D = \frac{\int_o^{\frac{\pi}{2}} C_{D\theta} d\theta}{\int_o^{\frac{\pi}{2}} d\theta} = \frac{2}{\pi} \int_o^{\frac{\pi}{2}} C_{D\theta} d\theta \tag{30}$$

or

$$\overline{C}_D = \frac{2}{\pi} \int_o^{\frac{\pi}{2}} \left\{\left[\tfrac{2}{3}(2 - K)\right] \sin^3 \theta + \left[0.714\tfrac{D}{L}(2 - K)\right] \cos^3 \theta\right\} d\theta \ . \tag{31}$$

Integrating,

$$\overline{C}_D = \left(0.283 + 0.303\tfrac{D}{L}\right)(2 - K) \ . \tag{32}$$

Random Tumbling -- Referring again to Figure 3, the average drag coefficient can be seen to be

$$\overline{C}_D = \frac{\int_o^{\frac{\pi}{2}} C_{D\theta}(2\pi \sin \theta) d\theta}{\int_o^{\frac{\pi}{2}} 2\pi \sin \theta \, d\theta} = \frac{1}{2\pi} \int_o^{\frac{\pi}{2}} C_{D\theta}(2\pi \sin \theta) d\theta \ . \tag{33}$$

Substituting Equation 29 into Equation 33,

$$\overline{C}_D = \int_o^{\frac{\pi}{2}} \left\{\left[\tfrac{2}{3}(2 - K)\right] \sin^4 \theta + \left[0.714\tfrac{D}{L}(2 - K)\right] \sin \theta \cos^3 \theta\right\} d\theta \ . \tag{34}$$

Integrating,

$$\bar{C}_D = \left[\left(\frac{2}{3}\{2 - K\}\right)\left(\frac{3}{8}\theta - \frac{\sin 2\theta}{4} + \frac{\sin 4\theta}{32}\right) + \left(0.714\,\frac{D}{L}\{2 - k\}\right)\left(-\frac{\cos^4\theta}{4}\right)\right]_0^{\frac{\pi}{2}} \quad (35)$$

$$\bar{C}_D = \left(0.393 + 0.178\frac{D}{L}\right)(2 - K) \ . \quad (36)$$

Heating Ratios

Trajectory computer programs such as the TTA program[4] are capable of calculating continuum-flow heating rates to the stagnation point of a sphere ($\dot{q}_{ss}\sqrt{R}$) entering on the same trajectory as the vehicle in question. Because of the relative ease of obtaining $\dot{q}_{ss}\sqrt{R}$, it is desirable to find a relation between local heating rates and $\dot{q}_{ss}\sqrt{R}$. For equilibrium continuum laminar flow and velocities below 25,000 ft/sec, the ratios of local to stagnation heating remain fairly constant. This ratio, which will be used for continuum flow, is defined as

$$F_q = \frac{\text{local heating rate}}{\text{stagnation heating to a 1-ft-radius sphere}} \text{ (dimensionless)}.$$

A similar situation exists for free-molecular flow. It is convenient to calculate free-molecular heating to a flat plate perpendicular to flow and to use these heating rates as a reference. Then local or average heating rates can be found by ratioing them to this reference. For most shapes, this ratio remains almost constant for Mach numbers greater than 10. One notable exception is heating to surfaces parallel to flow, where the heating ratio is strongly dependent on Mach number. The free-molecular heating ratios used in this report are defined as:

$$F_{FM} = \frac{\text{local heating rate}}{\text{heating rate to flat plate perpendicular to flow}} \text{ (dimensionless)}.$$

Free-Molecular Flow

A good approximation of free-molecular heating to a flat plate perpendicular to flow can be found by using the product of the accommodation coefficient, the stagnation enthalpy, and the mass-flow rate. In equation form,

$$\dot{q}_\perp = aH_o(\rho_\infty V_\infty)$$

$$\dot{q}_\perp = \frac{a\rho_\infty V_\infty^3}{2J} = \frac{a\rho_\infty V_\infty^3}{1556}\left(\frac{\text{BTU}}{\text{ft}^2\ \text{sec}}\right). \quad (38)$$

The accommodation coefficient is defined by

$$a = \frac{E_i - E_r}{E_i - E_w} \ , \quad (39)$$

where

E_i = energy brought to the wall by incident molecules
E_r = energy carried away by re-emitted molecules
E_w = energy that would be carried away if the re-emitted air were at wall temperature

Typical values of accommodation coefficients are given in Table I, which is taken from Reference 5.

TABLE I

Accommodation Coefficients

Surface	a
Aluminum, machined	0.95 - 0.97
Aluminum, polished	0.87 - 0.95
Cast iron, machined	0.87 - 0.88
Cast iron, polished	0.87 - 0.93
Bronze, machined	0.89 - 0.93
Bronze, polished	0.91 - 0.94
Flat black lacquer	0.88 - 0.89

Oppenheim[6] developed a more versatile method of calculating free-molecular heating, using kinetic theory. Oppenheim's final form of the heat-transfer equation is

$$\dot{q} = StC_{P_\infty}\rho_\infty gV_\infty(T_{aw} - T_w) \ , \tag{40}$$

where the Stanton number and recovery factor are solved for as a function of Mach number, specific heat ratio, accommodation coefficient, and configuration.

This equation will now be solved for the case of a flat plate perpendicular to flow, for use as a reference heating rate. It will be assumed that the specific heat ratio is 1.4, since most of the free-molecular heating during re-entry takes place at altitudes where most air molecules are diatomic. Referring to the perpendicular flat plate equations for Stanton number and recovery factor in Reference 6, and defining the molecular speed ratio as

$$s = M\sqrt{\frac{\gamma}{2}} \ , \tag{41}$$

$$\frac{1}{a}\frac{\gamma}{\gamma + 1}St = \frac{1}{4\sqrt{\pi}s}\left[e^{-s^2} + \sqrt{\pi}s(1 + erfs)\right] \ . \tag{42}$$

For Mach numbers greater than 2, Equation 42 is equal to a constant value of 0.500, so the Stanton number is

$$St = 0.856a \ , \tag{43}$$

and

$$\frac{\gamma + 1}{\gamma}r = \frac{2se^{-s^2} + (2s^2 + 1)\sqrt{\pi}(1 + erfs)}{s\left[e^{-s^2} + \sqrt{\pi}s(1 + erfs)\right]} \ . \tag{44}$$

For Mach numbers greater than 10, Equation 44 is equal to a constant value of 2.00, so the recovery factor is

$$r = 1.167 \ . \tag{45}$$

Equations 43 and 45 are now substituted into Equation 40 along with the appropriate equation for adiabatic wall temperature. The wall temperature is negligible compared to T_{aw} for most cases and will be omitted:

$$\dot{q}_{\perp} = 0.856 a C_{p_\infty} \rho_\infty g V_\infty T_\infty (1 + 0.233 M_\infty^2) \ , \tag{46}$$

but

$$M = \frac{V_\infty}{C} \tag{47}$$

and the speed of sound is

$$C = 49.1\sqrt{T_\infty} \ , \tag{48}$$

so that

$$\dot{q}_{\perp} = 0.856 a C_{p_\infty} \rho_\infty g V_\infty \left(T_\infty + \frac{V_\infty^2}{10,330} \right) \ . \tag{49}$$

Since T_∞ is much smaller than $(V_\infty^2)/(10,330)$ for re-entry velocities, T_∞ can be neglected in Equation 49, so that

$$\dot{q}_{\perp} = \frac{a C_{p_\infty} \rho_\infty g V_\infty^3}{12,070} = \frac{a C_{p_\infty} \rho_\infty V_\infty^3}{375} \left(\frac{BTU}{ft^2 \ sec} \right) \ . \tag{50}$$

For a specific heat of 0.241, which corresponds to a free-stream temperature of 190°F, Equation 50 is identical to Equation 38, so that for cool-walled vehicles at Mach numbers greater than 10, the simpler equation may be used.

Next, F_{FM} ratios will be developed for several basic shapes needed to calculate heating of a cylinder for the various modes of stable and tumbling re-entry.

For the sides of a rotating, side-on cylinder,

$$\frac{1}{a} \frac{\gamma}{\gamma + 1} St = \frac{e^{\frac{s^2}{2}}}{4\sqrt{\pi}} \left\{ \frac{1}{s} I_o\left(\frac{s^2}{2}\right) + s\left[I_o\left(\frac{s^2}{2}\right) + I_1\left(\frac{s^2}{2}\right) \right] \right\} \tag{51}$$

and

$$\frac{\gamma + 1}{\gamma} r = \frac{(2s^2 + 3)I_o\left(\frac{s^2}{2}\right) + (2s^2 + 1)I_1\left(\frac{s^2}{2}\right)}{(s^2 + 1)I_o\left(\frac{s^2}{2}\right) + s^2 I_1\left(\frac{s^2}{2}\right)} . \tag{52}$$

Solving Equation 40 using these two equations for Mach numbers from 5 to 40 and ratioing the results to $\dot{q}_\perp$ for the same Mach numbers generated the curve of F_{FM} versus Mach number shown in Figure 5.

For surfaces parallel to flow,

$$\frac{1}{a} \frac{\gamma}{\gamma + 1} St = \frac{1}{4\sqrt{\pi} s} \tag{53}$$

and

$$\frac{\gamma + 1}{\gamma} r = 2 . \tag{54}$$

Substituting these values into Equation 40 for Mach numbers from 3 to 40 and again ratioing the results to Equation 50 gives the F_{FM} curve shown in Figure 6.

For free-molecular flow on the back side of cylinders in cross flow, at Mach numbers greater than 5, the F_{FM} ratio was calculated to be less than 0.003, and the F_{FM} ratio for the back side of a flat plate is less than 0.0002. Therefore, all backside heating can be considered zero compared to heating of flow-impinging surfaces.

Oppenheim states that free-molecular heating to flat plates at angles of attack can be computed using the equations

$$St_\theta = (\sin \theta) St_\perp(\eta) \tag{55}$$

and

$$r_\theta = \frac{2\gamma}{\gamma + 1} \cos^2 \theta + (\sin^2 \theta) r_\perp(\eta) , \tag{56}$$

where $St_\perp(\eta)$ and $r_\perp(\eta)$ are computed replacing s with $\eta = s \sin \theta$.

This can be a laborious process, and for Mach numbers greater than 10 the results of Oppenheim's method can be approximated to within 0.5 percent by the equation

$$\dot{q}_\theta = \dot{q}_\perp(\sin \theta + 0.0113 \cos \theta) \text{ for } 0 \leq \theta \leq \frac{\pi}{2} , \tag{57}$$

and

$$\dot{q}_\theta = 0 \text{ for } -\frac{\pi}{2} \leq \theta < 0 . \tag{58}$$

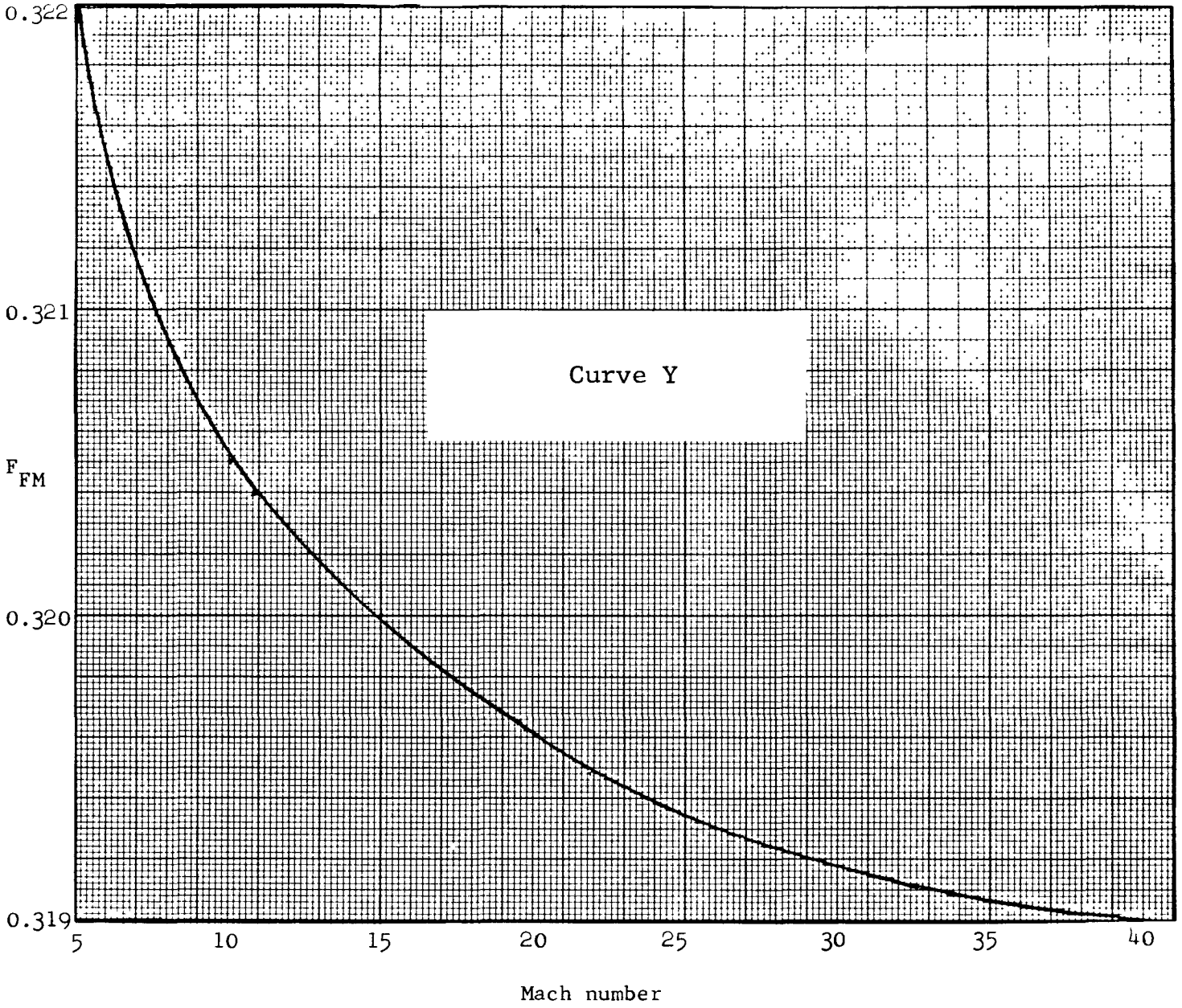

Figure 5. Free-molecular flow ratios of average heating on the sides of a rotating, side-on cylinder ($\theta = 90^{o}$) to heating on surfaces perpendicular to flow

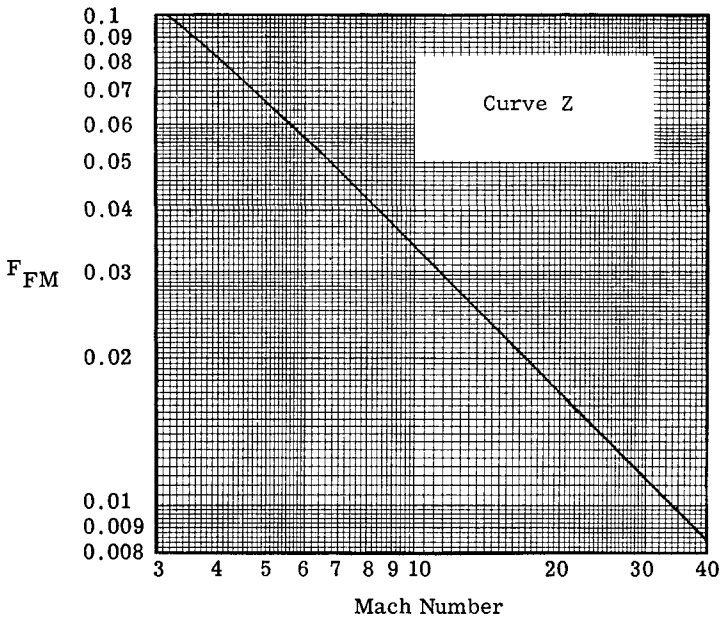

Figure 6. Free-molecular flow ratios of heating on surfaces parallel to flow to heating on surfaces perpendicular to flow

Equations 50, 57, and 58, and Figures 5 and 6 are all that will be necessary to compute the average free-molecular heating ratios for cylinders. To simplify the forthcoming equations, the F_{FM} of cross-flow cylinders (Figure 5) will be defined as Y and the F_{FM} for parallel flow (Figure 6) will be defined as Z.

Side-On and Spinning -- The average heating ratio to the side of the spinning cylinder has already been computed, and the values (Y) are given in Figure 5. The ends of the cylinder are parallel to flow, and the heating ratios (Z) are given in Figure 6.

End-On -- The sides of an end-on cylinder are parallel to flow and the heating ratios are Z (Figure 6). The front end of the cylinder is perpendicular to flow, so the heating ratio is 1. The heating ratio of the aft end is zero.

End-Over-End Tumbling and Spinning -- Free-molecular heating is a linear sin and cos function of angle of attack, as can be seen from Equation 57. Therefore, the heating ratio for the sides of a cylinder as a function of angle of attack (see Figure 2) is

$$F_{FM\theta} = Y \sin \theta + Z \cos \theta \ , \qquad (59)$$

and the average heating ratio to the sides is given by

$$\overline{F}_{FM} = \frac{\int_o^{\frac{\pi}{2}} F_{FM\theta} d\theta}{\int_o^{\frac{\pi}{2}} d\theta} \tag{60}$$

$$\overline{F}_{FM} = \frac{2}{\pi} \int_o^{\frac{\pi}{2}} (Y \sin \theta + Z \cos \theta) d\theta \tag{61}$$

$$\overline{F}_{FM} = 0.637 \ (Y + Z) \ . \tag{62}$$

For each end, the average ratio can be found using Equations 57 and 58:

$$\overline{F}_{FM} = \frac{\int_o^{\frac{\pi}{2}} (\sin \theta + 0.0113 \cos \theta) d\theta}{\int_o^{\pi} d\theta} \ . \tag{63}$$

Performing the integration,

$$\overline{F}_{FM} = 0.322 \ . \tag{64}$$

Random Tumbling and Spinning -- For the sides of the cylinder, the heating ratio as a function of angle of attack is again given by Equation 59. Referring to Figure 3, the average ratio can be seen to be

$$\overline{F}_{FM} = \frac{\int_o^{\frac{\pi}{2}} 2\pi \sin \theta \ (Y \sin \theta + Z \cos \theta) d\theta}{\int_o^{\frac{\pi}{2}} 2\pi \sin \theta \ d\theta} \ . \tag{65}$$

Integrating,

$$\overline{F}_{FM} = \left[Y\left(\frac{1}{2}\theta - \frac{1}{4} \sin 2\theta\right) + Z\left(\frac{1}{2} \sin^2 \theta\right) \right]_o^{\frac{\pi}{2}} \tag{66}$$

$$\overline{F}_{FM} = 0.785Y + 0.500Z \ . \tag{67}$$

For each end during random tumbling,

$$\bar{F}_{FM} = \frac{\int_0^{\frac{\pi}{2}} 2\pi \sin\theta \,(\cos\theta + 0.0113 \sin\theta)\,d\theta}{\int_0^{\pi} 2\pi \sin\theta \, d\theta} \tag{68}$$

or

$$\bar{F}_{FM} = \frac{1}{2}\int_0^{\frac{\pi}{2}} (\sin\theta \cos\theta + 0.0113 \sin^2\theta)\,d\theta \; ; \tag{69}$$

hence,

$$F_{FM} = 0.255 \; . \tag{70}$$

Continuum Flow

Convective heating rates to the stagnation point of a sphere can be found by[7]

$$\dot{q}_{ss} = \frac{17,600}{\sqrt{R}} \left(\frac{\rho_\infty}{\rho_s}\right)^{0.5} \left(\frac{V_\infty}{V_c}\right)^{3.15} \left(\frac{BTU}{ft^2 \; sec}\right) \; . \tag{71}$$

Equation 71, using a 1-foot nose radius, will be used as a reference heating rate for all heating ratios in this section.

It will now be necessary to determine the heating ratios $\left((\bar{\dot{q}})/(\dot{q}_{ss})\right)$ for the sides and ends of a cylinder versus angle of attack in order to compute average heating ratios for tumbling, spinning cylinders.

The distribution of heat transfer as a function of α around a cylinder in cross flow ($\theta = 90°$) is shown in Figure 7. The curve represents the ratio of local to stagnation-line heating. This is the distribution derived for a hemisphere by Kemp, Rose, and Detra[8], based on Lee's theory[9] for non-Newtonian pressure distributions. The curve has been extrapolated between $\alpha = 90°$ and 180°. Although this distribution is for a hemisphere, Zakkay and Visich[10] show that there is very little difference between the heat-transfer distribution around a sphere and a cylinder for $0° \leq \alpha \leq 90°$.

As shown by Lin[11], the ratio of convective heating at the stagnation line of a cylinder in cross flow to the convective heating at the stagnation point of a sphere of the same radius and wall temperature and under identical free-stream flow conditions is 0.747. Hence, the average heating ratio $\left((\bar{\dot{q}})/(\dot{q}_{ss})\right)$ to the side of a cylinder in cross flow can be found by

$$\frac{\bar{\dot{q}}}{\dot{q}_{ss}} = 0.747 \, \frac{\int_0^{\pi} \left(\frac{\bar{\dot{q}}}{\dot{q}_{sL}}\right) d\theta}{\int_0^{\pi} d\theta} \; . \tag{72}$$

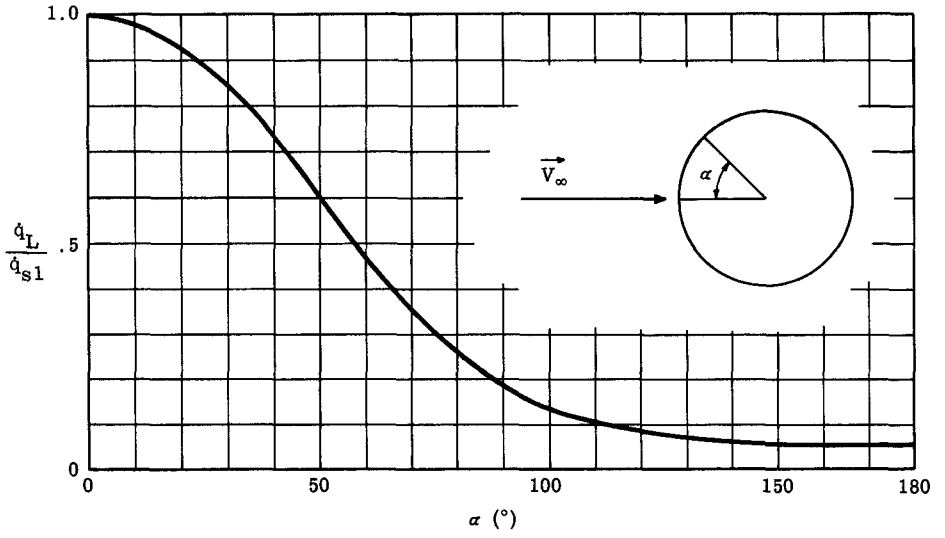

Figure 7. Ratio of local to stagnation-line heating on a cylinder in cross flow (θ = 90°)

Integrating the curve in Figure 7 numerically yields

$$\frac{\bar{\dot{q}}}{\dot{q}_{ss}} = 0.269 \ . \tag{73}$$

Figure 8 shows the ratio of the local heating to the side of an end-on cylinder (θ = 0°) to the stagnation-point heating. This curve is a compilation of data from various test series. The ratio of stagnation-point heating to an end-on cylinder to the stagnation-point heating of a sphere of the same radius is 0.5, so local heating ratios along the side of the cylinder can be obtained by dividing the values given in Figure 8 by 2. Integrating the curve in Figure 8 for L/D ratios up to 20 and dividing by the period of integration and by 2 gives the average heating ratios $((\bar{\dot{q}})/(\dot{q}_{ss}))$ for the sides of an end-on cylinder. The value of the curve in Figure 9, which shows $(\bar{\dot{q}})/(\dot{q}_{ss})$ as a function of the fineness ratio (L/D), will be referred to in future discussions as B for simplicity.

The heating distribution across the leading face of an end-on cylinder (θ = 0°) has been determined experimentally numerous times (References 3, 8, and 12). A distribution which approximates the average of the available data is illustrated in Figure 10. This curve can be expressed mathematically as

$$\frac{\dot{q}_L}{\dot{q}_{sp}} = 1.0 + 0.6\left(\frac{X}{R}\right)^{3.3} . \tag{74}$$

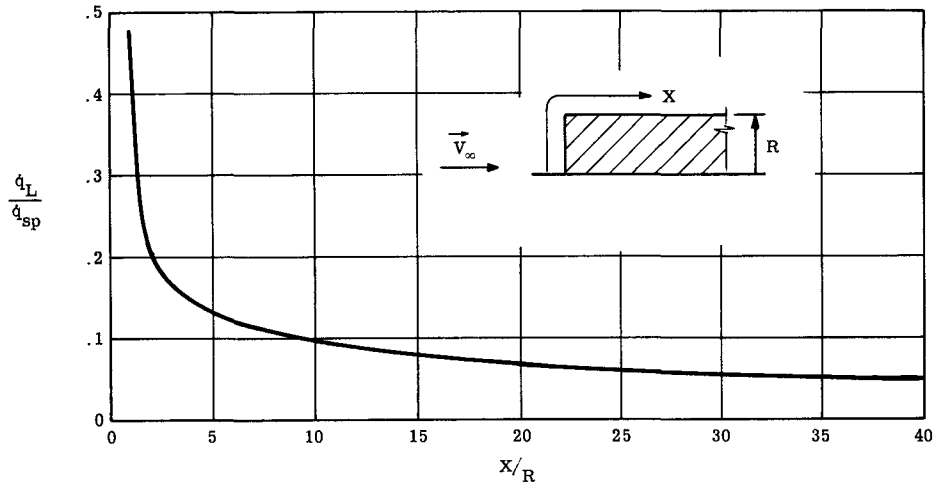

Figure 8. Ratio of local heating on the sides of an end-on cylinder to the stagnation-point heating (θ = 0°)

Integrating Equation 74 over the end of the cylinder and dividing by the surface area yields the average heating ratio to the end of the cylinder:

$$\frac{\bar{\dot{q}}}{\dot{q}_{sp}} = \frac{\int_0^R \left[1.0 + 0.6\left(\frac{X}{R}\right)^{3.3}\right] 2\pi x dx}{\pi R^2} = 1.226 \ . \tag{75}$$

Recall that

$$\frac{\dot{q}_{sp}}{\dot{q}_{ss}} = 0.5 \ . \tag{76}$$

The average heating ratio $(\bar{\dot{q}})/(\dot{q}_{ss})$ for the leading end of a cylinder at θ = 0° is

$$\frac{\bar{\dot{q}}}{\dot{q}_{ss}} = 0.5 \times 1.226 = 0.613 \ . \tag{77}$$

Weisblatt[13] reports on shock-tube and shock-tunnel tests conducted for the purpose of determining the average heating ratios on discs (analogous to the end of a cylinder) at angles of attack (θ) from 0° to 60°. The results of hot-shot tunnel tests at Mach numbers from 9.4 to 19.0 (Reference 12) and angles of attack from 0° to 30° agree with the data given in Reference 13. The test data were extrapolated past θ = 60° by calculating heating rates at θ = 90°, using laminar flat-plate theory and using a heating rate at θ = 180° which was 0.05 times the heating rate at θ = 0°.[14,15] These data are presented in Figure 11, which shows the ratio of the average heating to the end of a cylinder at angles of attack from 0° to 180° to the average heating at 0° angle of attack. Multiplying the values from Figure 11 by 0.613 (Equation 77) gives the $(\bar{\dot{q}})/(\dot{q}_{ss})$ ratios for the ends of cylinders at any angle of attack.

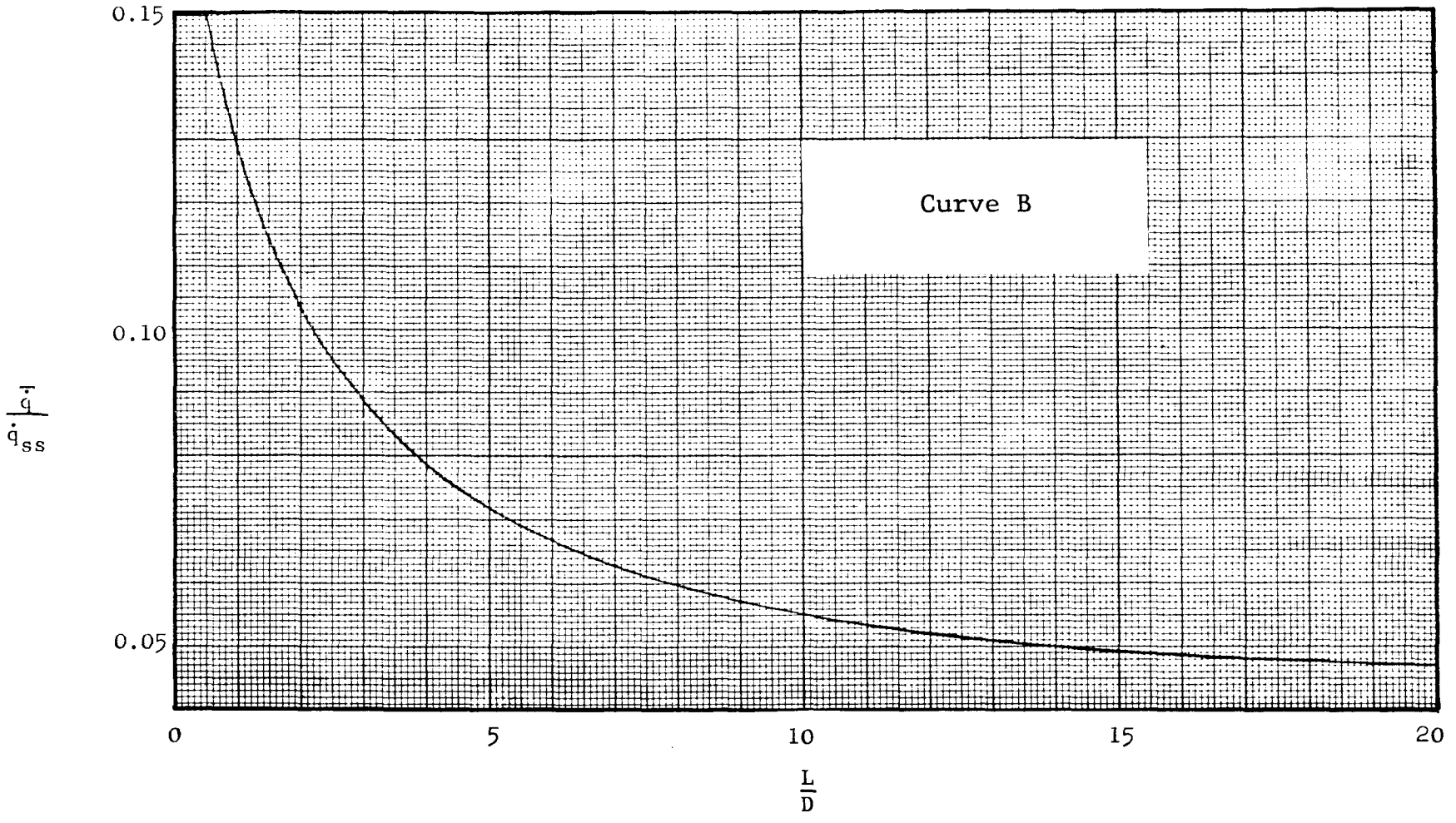

Figure 9. Ratio of average heating to the side of an end-on cylinder ($\theta = 0^{o}$) to stagnation-point heating to a sphere of the same radius

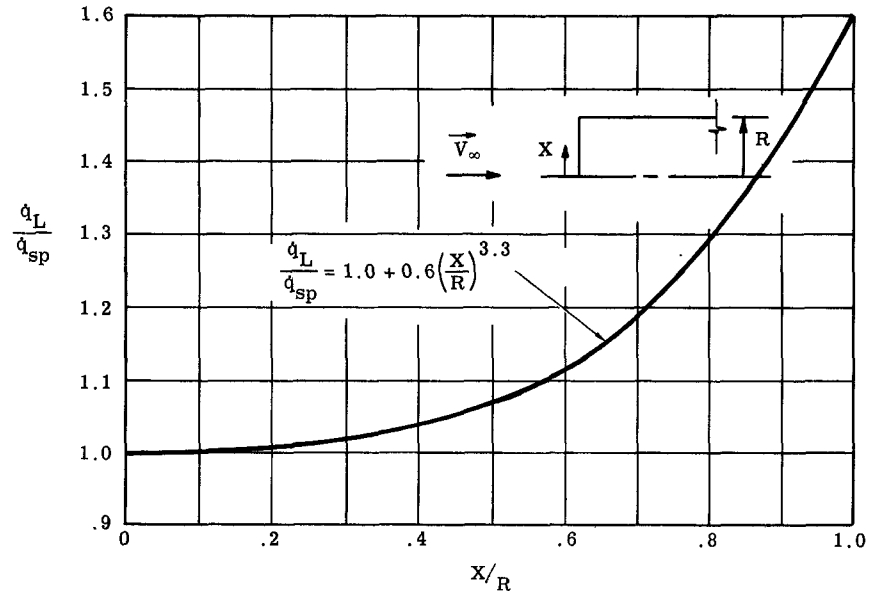

Figure 10. Ratio of local heating to stagnation-point heating on the front end of an end-on cylinder (θ = 0°)

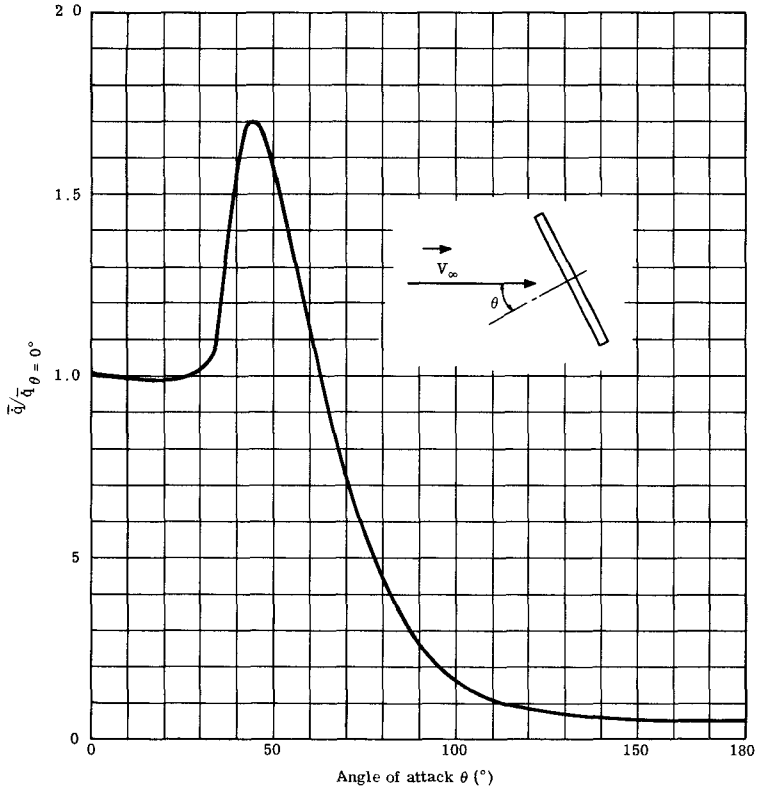

Figure 11. Ratio of heat transfer to a disc at angles of attack to heat transfer at 0° angle of attack

With the information from Equations 71, 73, and 77 and Figures 9 and 11, it is now possible to compute $\overline{F}_q$ ratios for the ends and sides of tumbling and stable cylinders. From Equation 71 and the definition of $\overline{F}_q$, it is obvious that all $\overline{F}_q$ ratios will include the term $(R)^{-1/2}$ as well as a shape factor.

Side-On and Spinning -- For the sides of a spinning cylinder at $\theta = 90°$, $\overline{F}_q$ is found using Equation 73:

$$\overline{F}_q = \frac{1}{\sqrt{R}}(0.269) \quad . \tag{78}$$

The heating ratio for the ends of the cylinder can be found by multiplying the value from Figure 11 at $\theta = 90°$ by 0.613 (Equation 77):

$$\overline{F}_q = \frac{1}{\sqrt{R}}(0.613)(0.24) = \frac{1}{\sqrt{R}}(0.147) \quad . \tag{79}$$

End-On -- The average heating ratio to the sides of an end-on cylinder ($\theta = 0°$) is given in Figure 9 as a function of L/D so that

$$\overline{F}_q = \frac{1}{\sqrt{R}}(B) \quad . \tag{80}$$

The average heating ratio to the front end of the cylinder has been given in equation 77:

$$\overline{F}_q = \frac{1}{\sqrt{R}}(0.613) \quad . \tag{81}$$

The average heating ratio to the aft end can be found by multiplying Equation 81 by the value shown in Figure 11 for $\theta = 180°$. Therefore,

$$\overline{F}_q = \frac{1}{\sqrt{R}}(0.0307) \quad . \tag{82}$$

End-Over-End Tumbling and Spinning -- To date there is very little knowledge about heat transfer to yawed cylinders. Several tests have been performed to study the effects of angle of attack on aero heating along the stagnation line of cylinders.[13,16,17] Reference 16 indicates that for supersonic flow the stagnation-line heating varies as $\sin\theta$, whereas Reference 17 suggests that for hypersonic flow the stagnation-line heating curve would have a lower value varying as $\sin^{3/2}\theta$. The data presented in Reference 13 for the sides of a yawed cylinder (Mach 11.5 and angles of attack from 30° to 90°), along with heating ratios for 0° angle of attack taken from Figure 9, can best be fitted by the following curve.

$$\frac{\overline{\dot{q}}}{\dot{q}_{ss}} = (\text{average heating ratio at } 0° \text{ angle of attack})(\cos^2\theta) + (\text{average heating ratio at } 90° \text{ angle of attack})(\sin^2\theta) \quad . \tag{83}$$

The distribution for heating to the sides of a cylinder given in Equation 83 will be used for the remainder of this report.

Referring to Figure 2, Equations 73 and 83 and Figure 9, the average heating ratio ($\overline{F}_q$) to the sides of an end-over-end tumbling and spinning cylinder can be seen to be

$$\overline{F}_q = \frac{\frac{1}{\sqrt{R}} \int_o^{\frac{\pi}{2}} (0.269 \sin^2 \theta + B \cos^2 \theta) d\theta}{\int_o^{\frac{\pi}{2}} d\theta} . \tag{84}$$

Performing the integration,

$$\overline{F}_q = \frac{2}{\pi\sqrt{R}} \left[0.269 \left(\frac{1}{2}\theta - \frac{1}{4} \sin 2\theta \right) + B \left(\frac{1}{2}\theta + \frac{1}{4} \sin 2\theta \right) \right]_o^{\frac{\pi}{2}} \tag{85}$$

$$\overline{F}_q = \frac{1}{\sqrt{R}} (0.134 + 0.500B) . \tag{86}$$

The average heating ratio to the ends of an end-over-end tumbling cylinder can be found by numerically integrating the curve in Figure 11 and dividing by the period of integration, then multiplying the result by $1/\sqrt{R}$ and 0.613 (Equation 77). Hence,

$$\overline{F}_q = \frac{1}{\sqrt{R}} (0.538)(0.613) = \frac{1}{\sqrt{R}} 0.329 . \tag{87}$$

Random Tumbling and Spinning -- Using a method similar to that used for end-over-end tumbling but referring to Figure 3, the average heating ratio ($\overline{F}_q$) for the sides of a randomly tumbling and spinning cylinder can be found by the following equation:

$$\overline{F}_q = \frac{\frac{1}{\sqrt{R}} \int_o^{\frac{\pi}{2}} (0.269 \sin^2 \theta + B \cos^2 \theta)(2\pi \sin \theta) d\theta}{\int_o^{\frac{\pi}{2}} 2\pi \sin \theta \, d\theta} \tag{88}$$

$$\overline{F}_q = \frac{1}{\sqrt{R}} \left[0.269 \left(-\frac{1}{3} \cos \theta \sin^2 \theta - \frac{2}{3} \cos \theta \right) + B \left(-\frac{\cos^3 \theta}{3} \right) \right]_o^{\frac{\pi}{2}} \tag{89}$$

$$\overline{F}_q = \frac{1}{\sqrt{R}} (0.179 + 0.333B) . \tag{90}$$

The curve in Figure 11 for the average heating ratio to the end of a cylinder versus angle of attack can be approximated by the following equations:

$$\frac{\bar{\dot{q}}}{\bar{\dot{q}}_{\theta=0}} = 1.0 , \qquad 0 \leq \theta < \frac{\pi}{6} ; \tag{91a}$$

$$\frac{\bar{\dot{q}}}{\bar{\dot{q}}_{\theta=0}} = -0.4 + \frac{8.4}{\pi}\theta , \qquad \frac{\pi}{6} \leq \theta < \frac{\pi}{4} ; \tag{91b}$$

$$\frac{\bar{\dot{q}}}{\bar{\dot{q}}_{\theta=0}} = 3.3 - \frac{6.4}{\pi}\theta , \qquad \frac{\pi}{4} \leq \theta < \frac{\pi}{2} ; \tag{91c}$$

$$\frac{\bar{\dot{q}}}{\bar{\dot{q}}_{\theta=0}} = 0.1 , \qquad \frac{\pi}{2} \leq \theta \leq \pi . \tag{91d}$$

Using Equations 77 and 91, the average heating ratio ($\bar{F}_q$) for the end of a randomly tumbling cylinder can be found by

$$\bar{F}_q = \frac{0.613}{\sqrt{R}} \frac{\sum_{i=o}^{\pi} \int_i (2\pi \sin\theta)\left(\frac{\bar{\dot{q}}}{\bar{\dot{q}}_{\theta=0}}\right) d\theta}{\int_o^{\pi} 2\pi \sin\theta \, d\theta} . \tag{92}$$

Substituting for $\frac{\bar{\dot{q}}}{\bar{\dot{q}}_{\theta=0}}$,

$$\bar{F}_q = \frac{0.306}{\sqrt{R}}\left[\int_o^{\frac{\pi}{6}} \sin\theta \, d\theta + \int_{\frac{\pi}{6}}^{\frac{\pi}{4}} \left(-0.4 + \frac{8.4}{\pi}\theta\right)\sin\theta \, d\theta + \right.$$

$$\left. \int_{\frac{\pi}{4}}^{\frac{\pi}{2}} \left(3.3 - \frac{6.4}{\pi}\theta\right) \sin\theta \, d\theta + \int_{\frac{\pi}{2}}^{\pi} 0.1 \sin\theta \, d\theta \right] . \tag{93}$$

Integrating,

$$\bar{F}_q = \frac{1}{\sqrt{R}}(0.323) . \tag{94}$$

Transition from Free-Molecular to Continuum Flow

Flow in the various transition regimes between free-molecular and continuum is extremely complicated, and no satisfactory theoretical solution has yet been offered. Therefore, no detailed development of drag coefficients or heating rates will be presented in this report for transition flow. However, several methods will be presented for calculating the limits of free-molecular and continuum flows and for extrapolating drag coefficients and heating rates between these two relatively well-defined regimes.

Tsien[18,19] defined the limits of the transition regimes by using a Knudsen number based on free-stream mean free path (λ_∞) and boundary-layer thickness (δ). The following relation for mean free path was derived by kinetic theory·

$$\lambda_\infty = 1.255\frac{\mu_\infty\sqrt{\gamma_\infty}}{\rho_\infty C_\infty} \quad . \tag{95}$$

Defining Knudsen number as

$$K_n = \frac{\lambda_\infty}{\delta} \quad . \tag{96}$$

Combining Equations 95 and 96,

$$K_n = 1.255\sqrt{\gamma_\infty}\frac{M_\infty}{Re_\delta} \quad . \tag{97}$$

Expressing Reynolds number in terms of characteristic body length,

$$K_n = 1.255\sqrt{\gamma_\infty}\frac{M_\infty}{Re_L}\frac{L}{\delta} \quad . \tag{98}$$

For extremely low Reynolds numbers corresponding to near free-molecular transition flow,

$$\frac{L}{\delta} \approx 1 \quad , \tag{99}$$

so that

$$K_n = 1.255\sqrt{\gamma_\infty}\frac{M_\infty}{Re_L} \quad . \tag{100}$$

Taking K_n to be approximately 10 between free-molecular and transition flow, free-molecular flow exists when

$$\frac{M_\infty}{Re_L} > 10 \quad . \tag{101}$$

For larger Reynolds numbers and continuum flow,

$$\frac{L}{\delta} = 0.215\sqrt{Re_L} \tag{102}$$

for laminar flow and

$$\frac{L}{\delta} = 2.66 Re_L^{0.2} \tag{103}$$

for turbulent flow. Substituting Equations 102 and 103 into 98,

$$Kn_{Lam} = 0.27\sqrt{\gamma_\infty}\frac{M_\infty}{\sqrt{Re_L}} \tag{104}$$

and

$$Kn_{Turb} = 3.33\sqrt{\gamma_\infty}\frac{M_\infty}{Re_L^{0.8}} . \tag{105}$$

For a limiting Knudsen number of 0.003, laminar continuum flow would exist when

$$\frac{M_\infty}{\sqrt{Re_L}} < 0.01 . \tag{106}$$

If conditions exist such that transition would be to turbulent flow, continuum flow would exist when

$$\frac{M_\infty}{Re_L^{0.8}} < 0.0008 . \tag{107}$$

The realms of flow defined by Equations 101, 106, and 107 are shown on a Mach-Reynolds number field in Figure 12.

Whereas the preceding discussion based Knudsen number on free-stream mean free path, Probstein[20] offered an alternate method using the mean free path at the wall of the vehicle. With the coordinate system fixed in the vehicle,

$$\lambda_w = \frac{4}{\sqrt{\pi\gamma_\infty}}\left(\frac{T_w}{T_\infty}\right)^{0.5}\left(\frac{\lambda_\infty}{M_\infty}\right) \tag{108}$$

in the free-molecular regime.

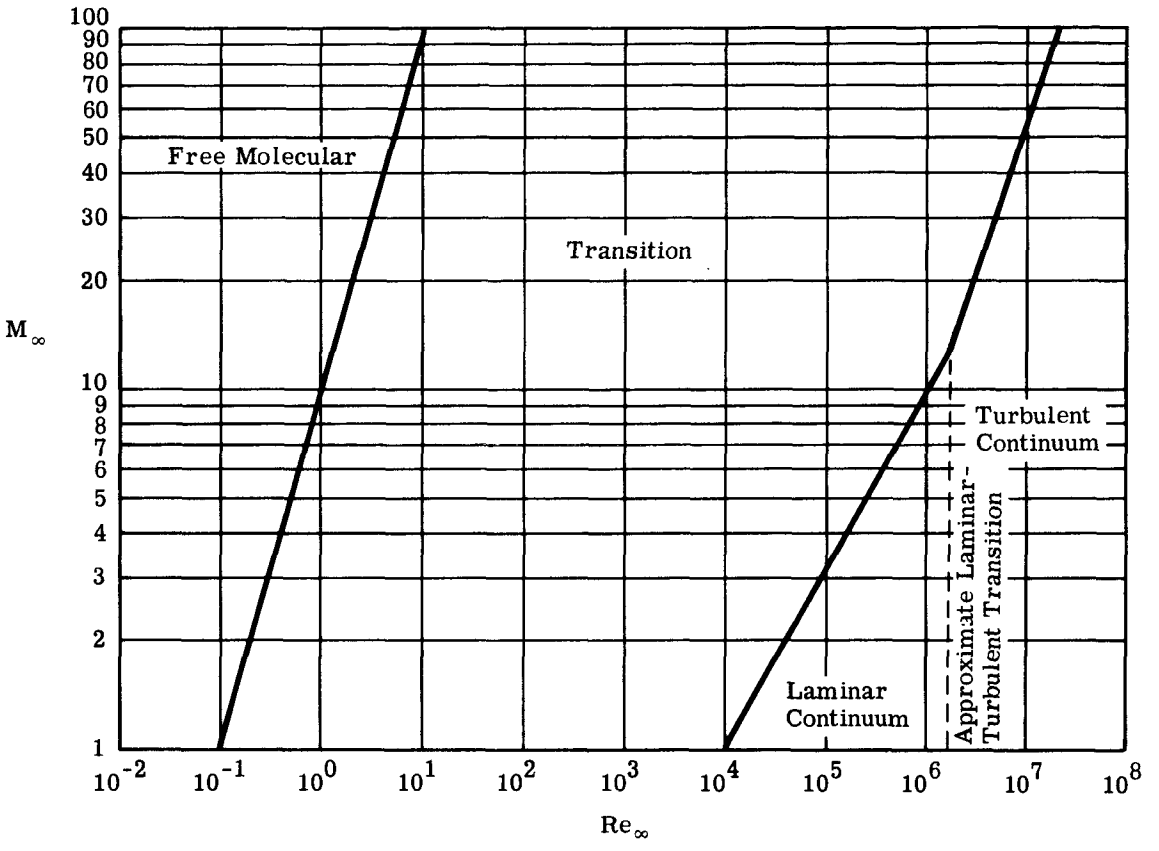

Figure 12. Flow regimes in Mach-Reynolds field

Using body radius as the critical dimension in Knudsen number, the limiting K_n for free-molecular flow was calculated to be 10, so the vehicle is in free-molecular flow when

$$\frac{\lambda_\infty}{R} > 4.43\sqrt{\gamma_\infty}\left(\frac{T}{T_w}\right)^{0.5} M_\infty \, . \tag{109}$$

The limit of continuum flow for the nose regions of blunt bodies was found using the relationship

$$\frac{\lambda_2}{\Delta} \ll 1 \, , \tag{110}$$

where

λ_2 = mean free path behind the shock
Δ = shock stand-off distance.

From Equation 110 the criterion for continuum flow was computed to be

$$\frac{\lambda_\infty}{R} < 0.1K \ , \tag{111}$$

K being the density ratio across the shock wave (ρ_∞/ρ_2).

With the limits of the transition regimes defined, it is now necessary to find a way to extrapolate drag coefficients and heating rates between free-molecular and continuum flow. Experiments conducted in a hot-shot tunnel on spheres, blunt cones, sharp cones, normal discs, and inverted hemispheres[21] showed that drag coefficients are an exponential function of Knudsen number in transition flow:

$$C_D \propto \ln(K_n) \ , \tag{112}$$

but

$$\lambda \propto \frac{1}{\rho} \ , \tag{113}$$

so

$$C_D \propto \ln \frac{1}{\rho} \ . \tag{114}$$

Density is proportional to e^{-h}. Therefore C_D varies approximately linearly with altitude between the free-molecular and continuum flow regimes.

Heating ratios in the transition region are not as easily defined as drag coefficients. Except for areas near the stagnation point, a good approximation to transition heating can be obtained for leading surfaces by extending free-molecular and continuum heating curves to their intersection, as shown in Figure 13, curve ABD. Since most of the heating to a tumbling vehicle takes place on the areas which are instantaneously facing forward, this method may also be used for tumbling cylinders. The results of this method are not only quite close to the various theories for transition heating[20,22,23] and low-density wind-tunnel tests[21,22,24], but also agree with flight-test data from Sandia's Re-entry Flight Demonstration Number 2 (RFD-2).

Near the stagnation point, heating rates are up to 30-percent higher than those predicted by continuum theory during the vorticity interaction and viscous layer flow regimes of the transition region. This increase occurs when the boundary layer thickness is of the same order as the shock layer thickness. Vorticity interaction becomes important when the vorticity in the inviscid layer due to the shock wave approaches the value of the vorticity in the boundary layer due to shear stresses. By comparison to theories and tunnel tests[20,21,23,24], the actual heating curve near the stagnation point can best be matched by following the free-molecular heating curve to a point where it intersects a curve 1.3 times the value of continuum heating. From this point the vorticity effects decay as a power function (straight line on log-log paper) over two increasing orders of magnitude of Reynoles number to the value given by continuum theory. An example of this method for the stagnation point of a 1-foot-radius sphere is shown in Figure 13, curve ACD. This vorticity effect is noticeable only near the stagnation point. As shown in Reference 22, vorticity effects drop off rapidly, and at 60° from the stagnation point of a sphere the effects are negligible. This increase in heating was also noted at the stagnation point of the RFD-2 re-entry system.

As proof that using the intersection of the free-molecular and continuum heating curves as the transition point is independent of vehicle diameter, it will be postulated that continuum heating is proportional to free-molecular heating at transition.

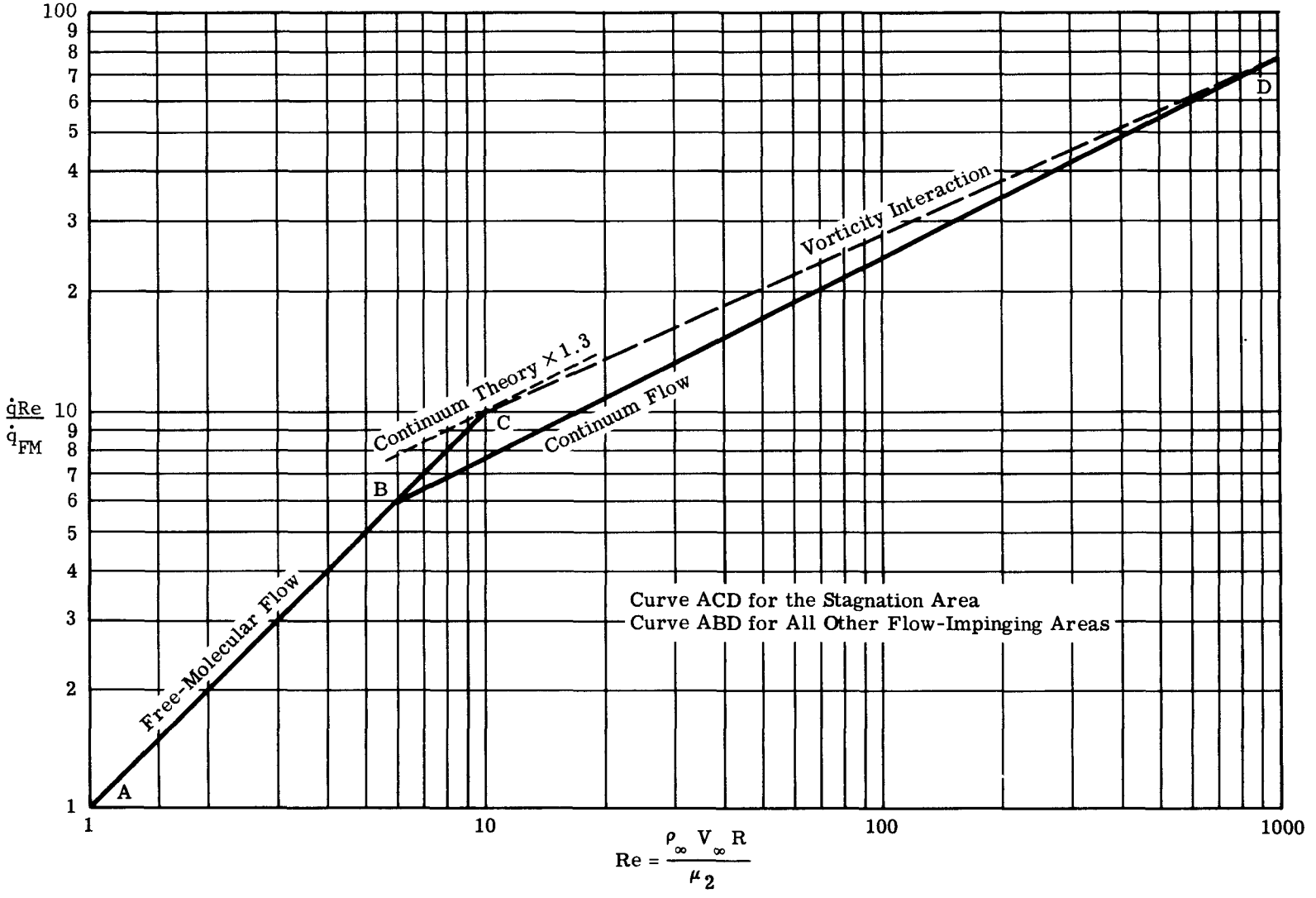

Figure 13. Effect of vorticity interaction during transition flow at the stagnation point of a 1-foot-radius sphere

Since

$$\text{continuum heating} \propto \left(\frac{\rho}{D}\right)^{0.5} \tag{115}$$

and

$$\text{free-molecular heating} \propto \rho \ , \tag{116}$$

then at transition

$$\frac{(\rho/D)^{0.5}}{\rho} = \text{constant} \ .$$

Simplifying,

$$\frac{1}{\rho D} = \text{constant} \ .$$

But $\lambda \propto 1/\rho$ during the altitude range in which transition usually takes place, so

$$\frac{\lambda}{D} = \text{constant} \ ,$$

or K_n equals a constant at transition, proving free-molecular heating remains proportional to continuum heating at transition, regardless of body diameter.

Summary

Drag coefficients and heating ratios were calculated for stable and unstable cylinders in free-molecular and continuum flow. The results are shown in Tables II and III.

TABLE II

C_D Based on $A_R = LD$

Case	Flow Regime	
	Free Molecular	Laminar Continuum
Side-on	2.0	$0.667(2 - K)$
End-on	$1.57\frac{D}{L}$	$0.714\frac{D}{L}(2 - K)$
End-over-end tumbling	$1.273 + \frac{D}{L}$	$(0.283 + 0.303\frac{D}{L})(2 - K)$
Random tumbling	$1.57 + 0.785\frac{D}{L}$	$(0.393 + 0.178\frac{D}{L})(2 - K)$

where

A_R = Reference area (ft^2)
D = Cylinder diameter (ft)
L = Cylinder length (ft)
K = Density ratio across a normal shock (ρ_∞/ρ_2)

TABLE III

Average Heating Ratios $\overline{F}_{FM}$ and $\overline{F}_q$

Case	Location	Flow Regime: Free Molecular, $\overline{F}_{FM}$	Flow Regime: Laminar Continuum, $\overline{F}_q$
Side-on and spinning	ends	Z	$\frac{1}{\sqrt{R}}(0.147)$
	sides	Y	$\frac{1}{\sqrt{R}}(0.269)$
End-on	front end	1	$\frac{1}{\sqrt{R}}(0.613)$
	aft end	0	$\frac{1}{\sqrt{R}}(0.0307)$
	sides	Z	$\frac{1}{\sqrt{R}}(B)$
End-over-end tumbling and spinning	ends	0.322	$\frac{1}{\sqrt{R}}(0.329)$
	sides	0.637(Y + Z)	$\frac{1}{\sqrt{R}}(0.134 + 0.500B)$
Random tumbling and spinning	end	0.255	$\frac{1}{\sqrt{R}}(0.323)$
	sides	0.785Y + 0.500Z	$\frac{1}{\sqrt{R}}(0.179 + 0.333B)$

where

$$\overline{F}_{FM} = \frac{\text{Average free-molecular heating rate}}{\text{Free-molecular heating rate to a plate perpendicular to flow}}$$

$$\overline{F}_q = \frac{\text{Average laminar continuum heating rate}}{\text{Stagnation-point heating rate to a 1-foot-radius sphere}}$$

$$Y = \frac{\text{Average free-molecular heating to a cylinder in cross flow}}{\text{Free-molecular heating to a plate perpendicular to flow}} \quad \text{(Figure 5)}$$

$$Z = \frac{\text{Free-molecular heating to a plate parallel to flow}}{\text{Free-molecular heating to a plate perpendicular to flow}} \quad \text{(Figure 6)}$$

$$B = \frac{\text{Average laminar continuum heating along the sides of an end-on cylinder}}{\text{Stagnation-point heating to a sphere of the same radius}} \quad \text{(Figure 9)}$$

R = Cylinder radius (ft)

The reference free-molecular heating rates can be found using

$$\dot{q}_{\perp} = \frac{a\rho_{\infty}V_{\infty}^3}{1556}\left(\frac{BTU}{ft^2\ sec}\right),$$

and the reference continuum heating rate may be obtained using

$$\dot{q}_{ss} = 17,600\left(\frac{\rho_\infty}{\rho_s}\right)^{0.5}\left(\frac{V_\infty}{V_c}\right)^{3.15}\left(\frac{\text{BTU}}{\text{ft}^2\ \text{sec}}\right).$$

Two methods of determining the limits of free-molecular and continuum flow were presented, and appear in Table IV.

TABLE IV

Limits of Free-Molecular and
Laminar Continuum Flow Regimes

Method	Free Molecular	Continuum
1	$\frac{M_\infty}{Re_L} > 10$	$\frac{M_\infty}{\sqrt{Re_L}} < 0.01$
2	$\frac{\lambda_\infty}{R} > 4.4\sqrt{\gamma_\infty}\left(\frac{T_\infty}{T_w}\right)^{0.5} M_\infty$	$\frac{\lambda_\infty}{R} < 0.1K$

Through the various transition regimes, drag coefficient can be extrapolated linearly with altitude between the two appropriate values from Table II.

A good approximation to heating rates in the transition regimes may be computed for tumbling cylinders and for flow-impinging surfaces of stable cylinders by extending free-molecular and continuum equations to their intersection. However, near the stagnation point of the vehicle, heating rates will be up to 30-percent higher than the computed values at this intersection, because of vorticity interaction. This increase decays over two increasing orders of magnitude of Reynolds number to the value given by continuum theory, as shown in Figure 13.

NOMENCLATURE

A = Area (ft^2)

A_R = Reference area (ft^2)

a = Accommodation coefficient

B = Value of curve in Figure 9

C_D = Drag coefficient

$\overline{C}_D$ = Average drag coefficient

c = Speed of sound (ft/sec)

c_p = Specific heat at constant pressure (BTU/lb °R)

D = Diameter (ft)

erf = Error function

$\overline{F}_{FM}$ = Ratio of average free-molecular heating to heating of a plate perpendicular to flow

$\overline{F}_q$ = Ratio of average laminar continuum heating to stagnation heating of a one-foor-radius sphere

g = 32.2 (ft/sec^2)

H = Enthalpy (BTU/lb)

h = Altitude (ft)

I_o = Bessel function of the first kind and zeroth order

I_1 = Bessel function of the first kind and first order

J = Mechanical equivalent of heat, 778 (ft-lb/BTU)

K = Density ratio across a normal shock, (ρ_∞/ρ_2) (see Reference 25)

K_n = Knudsen number

L = Length (ft)

M = Mach number

P = Pressure (lb/ft^2)

q = Dynamic pressure, $1/2\ \rho V^2$(lb/ft^2)

$\dot{q}$ = Heating rate ($BTU/ft^2 sec$)

$\overline{\dot{q}}$ = Average heating rate ($BTU/ft^2 sec$)

$\dot{q}_L$ = Local heating rate ($BTU/ft^2 sec$)

$\dot{q}_{sl}$ = Stagnation-line heating rate ($BTU/ft^2 sec$)

$\dot{q}_{sp}$ = Stagnation-point heating rate ($BTU/ft^2 sec$)

$\dot{q}_{ss}$ = Stagnation-point heating rate on a sphere ($BTU/ft^2 sec$)

R = Radius (ft)

R_e = Reynolds number

r = Recovery factor

St = Stanton number

s = Molecular speed ratio, $M\sqrt{\frac{\gamma}{2}}$

T = Temperature (°R)

V_c = Circular orbital velocity (gravitational acceleration x radius to center of earth)$^{1/2}$(ft/sec)

$\vec{V}_\infty$ = Free-stream velocity vector (ft/sec)

X = Distance along the surface of a cylinder

Y = Value of curve in Figure 5

Z = Value of curve in Figure 6

α = Radial angle with respect to the velocity vector (°)

γ = Specific-heat ratio

Δ = Shock stand-off distance (ft)

δ = Boundary-layer thickness (ft)

η = $S \sin \theta$

θ = Angle of attack (°)

λ = Mean free path of air molecules (ft)

μ = Viscosity (slug/ft-sec)

ρ = Air density (slug/ft^3)

ρ_s = Air density at sea level (slug/ft^3)

ϕ = Angle between a normal to the surface and the velocity vector (°)

Subscripts

A = Axial (end-on)

aw = Adiabatic wall

L = Based on characteristic length

o = Stagnation

T = Transverse (side-on)

w = Wall conditions

δ = Based on boundary-layer thickness

θ = As a function of angle of attack

∞ = Free stream

$\perp$ = Perpendicular to flow

2 = Downstream of a normal shock

LIST OF REFERENCES

1. Henry, I. G., "Lifetimes of Artificial Satellites of the Earth," Jet Propulsion Vol. 27, No. 1, 1957, pp 21-27.

2. Randall, D. E., A Method for Estimating the Drag Coefficient of Tumbling Circular Cylinder, Sandia Corporation, SC-TM-64-528, Unc. May 1964.

3. Stoney, W. E., Jr. and Swanson, A. G., Heat Transfer Measured on a Flat-Face Cylinder in Free Flight at Mach Numbers up to 13.9, NACA RM-L-57E13, June 17, 1957.

4. Allensworth, J. A. F., The TTA Generalized Rigid Body Theoretical Trajectory Program for Digital Computer, Sandia Corporation, SC-TM-64-526, Unc.

5. Truitt, R. W., Fundamentals of Aerodynamic Heating, Ronald Press Co., New York, 1960.

6. Oppenheim, A. K., "Generalized Theory of Convective Heat Transfer in a Free-Molecular Flow," Journal of the Aeronautical Sciences, January 1953.

7. Chapman, D. R., An Approximate Analytical Method for Studying Entry into Planetary Atmospheres, NASA, TR R-11, Unc, 1959.

8. Kemp, N., Rose, P., and Detra, R., "Laminar Heat Transfer Around Blunt Bodies in Dissociated Air," Journal of the Aerospace Sciences, July 1959.

9. Lees, L., "Laminar Heat Transfer Over Blunt-Nosed Bodies at Hypersonic Flight Speeds," Jet Propulsion, April 1956.

10. Zakkay, V. and Visich, M., "Pressure and Laminar Heat Transfer Distribution at the Nose Region of a Three-Dimensional Body," International Developments in Heat Transfer, Part II, ASME, 1961.

11. Lin, C., "Turbulent Flows and Heat Transfer," Volume V, High Speed Aerodynamics and Jet Propulsion, Princeton University Press, 1957.

12. Memo, Klett, R. D. 9312, to Clark, A. J., Jr., 9312, RFD-2 Aeroheating Hot Shot Tests Conducted at Rhodes & Bloxsom, October 8-12, 1963, Unc, November 21, 1963.

13. Research and Advanced Development Division, Aero Corp., Investigation of Re-entry Destruction of Nuclear Auxiliary Powerplants, AVCO, AVCO-RAD-TR-61-28, Unc, October 1961.

14. Powers, E. W., Stetson, K. F., Adams, M. C., A Shock Tube Investigation of Heat Transfer in the Wake of a Hemisphere-Cylinder, with Application to Hypersonic Flight, IAS-59-35, Unc, January 1959.

15. Larson, H. K., Heat Transfer in Separated Flows, IAS-59-37, Unc, January 1959.

16. Reshotko, E., and Beckwith, I., Compressible Laminar Boundary Layer Over a Yawed Infinite Cylinder With Heat Transfer and Arbitrary Prandtl Numbers, NACA-TN-3986, Unc, June 1957.

17. Eggers, A. J., Hansen, C. F., Cunningham, B. E., Theoretical and Experimental Investigation of the Effect of Yaw on Heat Transfer to Circular Cylinders in Hypersonic Flow, NACA-RM-A55E02, Unc, July 1955.

18. Tsien, H., "Superaerodynamics, Mechanics of Rarefied Gases," Journal of the Aeronautical Sciences, December 1946.

19. Eckert, E. R. G., Survey on Heat Transfer at High Speeds, MU-2214-ARL-189, Unc, December 1961

20. Probstein, R. F., "Shock Wave and Flow Field Development in Hypersonic Re-entry," A.R.S. Journal, February 1961.

21. Bloxsom, D. E., and Rhodes, B. V., "Experimental Effect of Bluntness and Gas Rarefaction on Drag Coefficients and Stagnation Heat Transfer on Axisymmetric Shapes in Hypersonic Flow," Journal of the Aerospace Sciences, December 1962.

22. Ferri, A., Zakkay, V., and Ting, L., Blunt Body Heat Transfer at Hypersonic Speeds and Low Reynolds Numbers, PIBAI-611, Unc, June 1960

23. Cheng, H., "Hypersonic Shock-Layer Theory of the Stagnation Region at Low Reynolds Numbers," The 1961 Heat Transfer and Fluid Mechanics Institute, Stanford Univ. Cal.

24. Ferri, A., and Zakkay, V., "Measurements of Stagnation Point Heat Transfer at Low Reynolds Numbers," Journal of the Aerospace Sciences, July 1962.

25. Wittliff, C. E., and Curtis, J. T., Normal Shock Wave Parameters in Equilibrium Air, C.A.L.-111, Unc. November 1961.

DISTRIBUTION:
H. G. Hembree, Safety Engineering & Test Branch, Division of Reactor Development, USAEC, Washington 25, D. C.
Lt. Col. W. K. Kern, Aerospace Safety Section, Engineering & Test Branch, Division of Reactor Development, USAEC, Washington 25, D. C.
S. A. Upson, Director, Reactor Operations Division, AEC Albuquerque Operations Office, P. O. Box 5400, Albuquerque, New Mexico
L. Otoski, Area Manager, AEC Albuquerque Operations Office, P. O. Box 5400, Albuquerque, New Mexico
C. R. Stahle, AEC New York Operations Office, New York, N. Y.
J. V. Levy, Area Manager, USAEC, Canoga Park Area Office, P. O. Box 591, Canoga Park, California, Attn: C. A. Malmstrom
R. L. Kirt, SNAP Program Director, Division of Reactor Development, USAEC, Washington 25, D. C.
T. B. Kerr, RNS, NASA Headquarters, Washington 25, D. C.
W. Hagis, Martin-Nuclear Co., Middle River, Maryland (2)
R. L. Detterman, Atomics International, P. O. Box 309, Canoga Park, California
Henry Hidalgo, Institute for Defense Analyses, 400 Army Navy Dr. Arlington, Va.
Glen Goodwin, NASA Ames Research Center, Moffett Field, California
Charles H. McLellan, NASA Langley Research Center, Langley Station, Hampton, Va.
S. P. Schwartz, 1
R. W. Henderson, 1000
J. P. Cody, 1320
J. W. Jones, 1510
R. S. Wilson, 1520
S. A. Moore, 1540
R. T. Othmer, 1541
B. E. Bader, 1541
B. M. Brake, 1541
P. L. Class, 1541
J. H. Scott, 1610
F. W. Neilson, 1620
C. Winter, 1630
A. V. Engle, 1632
E. H. Draper, 2000
D. R. Cotter, 5500
R. S. Claassen, 5100
J. D. Shreve, 5414
R. A. Bice, 7000
G. A. Fowler, 9000
D. B. Shuster, 9200
A. Y. Pope, 9300
H. E. Hansen, 9311
L. O. Cropp, 9311
R. N. Horton, 9311
B. W. Marshall, 9311
A. E. Stephenson, 9311
I. B. White, 9311
A. J. Clark, Jr., 9312
R. E. Berry, 9312
H. R. Spahr, 9312
R. M. Dayhoff, 9312
R. D. Klett, 9312 (8)
W. W. Roberts, 9312
J. W. McKiernan, 9319
L. C. Maydew, 9320
S. McAlees, 9321
M. L. Kramm, 9330
W. A. Jamieson, 8232
B. R. Allen, 3421
M. G. Randle, 3428-1, Bldg. 836
M. G. Randle, 3428-1, Bldg. 880
J. L. Fife, 3412 (2)
R. C. Smelich, 3427-3 (10)
T. B. Heaphy, 3411
For: DTIE (3)
H. F. Carroll (1)